Hybrid Tandem Photovoltaics

Emily Warren,[1] John Geisz,[1] Jeronimo Buencuerpo,[1]
Talysa Klein,[1] Bill McMahon,[1] Tim Silverman,[1]
Paul Stradins,[1] Kaitlyn VanSant,[1,2] Michelle Young,[1]
Riley Whitehead,[1] Mickey Wilson,[1] and Adele Tamboli[1]

1 National Renewable Energy Laboratory
2 Colorado School of Mines

NREL is a national laboratory of the U.S. Department of Energy
Office of Energy Efficiency & Renewable Energy
Operated by the Alliance for Sustainable Energy, LLC

This report is available at no cost from the National Renewable Energy Laboratory (NREL) at www.nrel.gov/publications.

Contract No. DE-AC36-08GO28308

Technical Report
NREL/TP-5900-84173
March 2023

Hybrid Tandem Photovoltaics

Emily Warren,[1] John Geisz,[1] Jeronimo Buencuerpo,[1]
Talysa Klein,[1] Bill McMahon,[1] Tim Silverman,[1]
Paul Stradins,[1] Kaitlyn VanSant,[1,2] Michelle Young,[1]
Riley Whitehead,[1] Mickey Wilson,[1] and Adele Tamboli[1]

1 National Renewable Energy Laboratory
2 Colorado School of Mines

Suggested Citation
Warren, Emily, John Geisz, Jeronimo Buencuerpo, Talysa Klein, Bill McMahon, Tim Silverman, Paul Stradins, Kaitlyn VanSant, Michelle Young, Riley Whitehead, Mickey Wilson, and Adele Tambol. 2023. *Hybrid Tandem Photovoltaics*. Golden, CO: National Renewable Energy Laboratory. NREL/TP-5900-84173.
https://www.nrel.gov/docs/fy23osti/84173.pdf

NREL is a national laboratory of the U.S. Department of Energy
Office of Energy Efficiency & Renewable Energy
Operated by the Alliance for Sustainable Energy, LLC

This report is available at no cost from the National Renewable Energy Laboratory (NREL) at www.nrel.gov/publications.

Contract No. DE-AC36-08GO28308

Technical Report
NREL/TP-5900-84173
March 2023

National Renewable Energy Laboratory
15013 Denver West Parkway
Golden, CO 80401
303-275-3000 • www.nrel.gov

NOTICE

This work was authored by the National Renewable Energy Laboratory, operated by Alliance for Sustainable Energy, LLC, for the U.S. Department of Energy (DOE) under Contract No. DE-AC36-08GO28308. Funding provided by the U.S. Department of Energy Office of Energy Efficiency and Renewable Energy Solar Energy Technologies Office. The views expressed herein do not necessarily represent the views of the DOE or the U.S. Government.

Final Technical Report (FTR)

Agency/Office/Program	DOE/EERE/Solar Energy Technology Office	
Award Number	DE-EE00034911	
Project Title	Hybrid Tandem Photovoltaics	
Principal Investigator	Emily Warren, Scientist Emily.Warren@nrel.gov 303-384-7293	
Business Contact	Daniel Friedman Daniel.Friedman@nrel.gov 303-384-6472	
Submission Date	September, 30, 2022	
DUNS Number	805948051 + 0000	
Recipient Organization	National Renewable Energy Lab	
Project Period	**Start:** 10/1/18	**End:** 6/30/22
Project Budget	Total $3M (DOE: $3M; C/S: $0)	
Submitting Official Signature	Signature	

1. **Acknowledgement:** "This material is based upon work supported by the U.S. Department of Energy's Office of Energy Efficiency and Renewable Energy (EERE) under Award Number(s) 34911."

2.

3. **Executive Summary:** Tandem solar cell structures are the only strategy demonstrated to surpass the detailed balance efficiency limit of high-quality single-junction solar cells. To continue to improve the efficiencies of cost-effective terrestrial solar power, hybrid tandems of dissimilar subcells are being considered by many around the world, especially designs that incorporate silicon solar cells as a bottom subcell. In this project, we studied a wide variety of tandem design possibilities including those with three-terminal (3T) and four-terminal (4T) configurations. The use of 3T and 4T designs could be useful for efficient and economical hybrid tandem designs that utilize the best available subcell materials such as emerging perovskite

materials. Three-terminal configurations, in particular, have not been sufficiently studied previously. We have laid the foundational groundwork in this project for understanding the operation of 3T tandems: developing a taxonomy for naming, a methodology for measuring and interconnecting, and models for simply characterizing 3T tandems. Electrical and optical subcell coupling between the subcells was also measured and modeled.

An important part of this work was the fabrication of novel example tandem structures, including 4T GaAs/Si, 3T GaInP/Si, 3T GaAs/Si, and 3T GaInP/GaAs devices. Using these high-quality tandem cells, we have been able to clearly demonstrate the achievability of high-efficiencies, and subtle physical effects such as photon recycling and luminescent coupling. We have developed and demonstrated essential building-block tools such as transparent conductive adhesives (TCA) and 3T silicon bottom cells with interdigitated back contacts (IBC) that can also be used in many other tandem designs. We have tested the reliability of these tools and devices under standardized testing and outdoor measurements. We have found 4T GaAs/Si tandems to be relatively straightforward to fabricate and robust in real-world outdoor conditions. While we have demonstrated working hybrid 3T III-V/TCA/Si IBC tandems, we experienced low yields even with our best process flows yet. Further work is still needed to improve the processing yield of these devices.

We therefore also created tandem cells using an all-III-V 3T tandem process which was very robust with high yields, allowing for the creation of voltage-matched strings in many different configurations using 8 nearly identical 3T tandems. Using these robust 3T tandem examples, we were able measure and precisely characterize 3T tandem behaviors to predict their operation under changing spectrum and temperature. The optoelectronic equivalent-circuit model was shown to be very general and applicable to hybrid tandems, and encompassed the operation 3T Si IBC cells. This general model has been distributed to the public in as open-source Python-based software called *PVcircuit*. We have calculated the implications of these new tandem device designs on the real-world energy production and shown how the relative performance of different tandem configurations is situational and can be engineered using the tools developed here.

This project has resulted in many peer reviewed publications [1-26] with one still under review [27]. The methods of 2T and 3T modeling and energy yield analysis have been published as open-source software [28] and one patent has been issued [29]. These publications, software, and IP are available to the public for further development of cost-effective energy solutions that will benefit all people.

4. Table of Contents:

5. Background:

The efficiency of traditional single junction photovoltaic (PV) technology is nearing its limit. Tandem/multijunction solar cells are able to convert sunlight to electricity with greater efficiency than single junction solar cells by splitting the solar spectrum across subcells with different bandgaps. For many years III-V multijunction solar cells have utilized two-terminal (2T) configurations for ease of use in space and concentrating photovoltaic (CPV) applications, but this requires careful material selection to achieve current-matching conditions for efficient operation. Four-terminal (4T) tandem configurations significantly expand the possibilities for efficient tandem material combinations because current-matching is not required as shown in Fig. 1 [30,31]. Ideally, a low-cost, high-quality top subcell could be paired with existing cheap and efficient silicon bottom subcells to create very efficient, economical utility-scale terrestrial tandem photovoltaics. [32,33] Three-terminal (3T) tandems [34-36] can also provide the design flexibility advantages of efficient 4T tandems without the disadvantages of shadow losses from intermediate metal grids, but also complicate the architecture of interconnecting cells into modules. [37-39] Since 3T and 4T tandems are not limited by current-matching, the energy yield over the course of time with varying spectra is likely to be improved over 2T tandems [40].

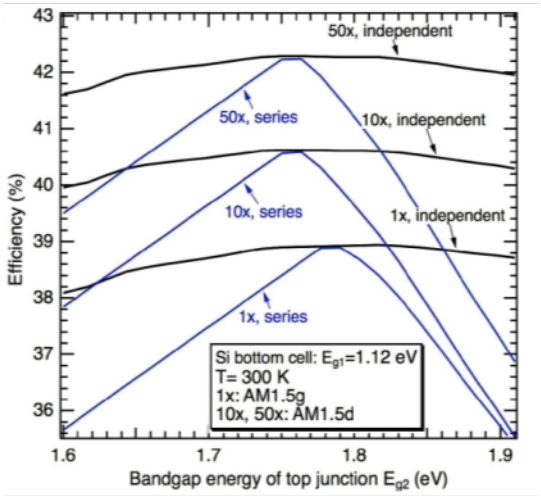

Figure 1 Modeled efficiencies of tandem solar cells with a Si bottom cell [30]. Series connected (2T) tandems are sensitive to current-matching, but independent subcells (e.g. 3T or 4T) are less sensitive to the top subcell bandgap

Recent progress with interdigitated back contact (IBC) silicon solar cells and transparent conductive adhesives (TCA) has enabled the conception of many possibilities for practical and economical 4T and 3T tandem designs. This project addresses challenges in interconnecting and scaling champion laboratory tandem cells to create strings and modules. Our experimental work focuses on demonstrating example III-V and Si tandem cells as model systems to understand how to fabricate and interconnect different tandem architectures (2T, 3T or 4T as shown in Fig. 2). We particularly focus on 3T tandems, which are the least understood approach to tandem cells, but have the potential to enable high energy yield and low-cost solar power relative to more traditional two and four terminal approaches. We have developed models for individual 3T subcells, and string-level simulations that can be applied to all absorber materials. We are also studying the reliability of tandem cells in an outdoor environment and long-term performance of novel cell components.

Previous collaborative work between NREL, Colorado School of Mines (CSM), Institute for Solar Energy Research in Hamelin (ISFH), École polytechnique fédérale de Lausanne (EPFL), and Swiss Center for Electronics and Microtechnology (CSEM) resulted in record device efficiencies and novel device geometries using a mechanically-stacked III-V/Si multijunction solar cell platform. First, we demonstrated four-terminal III-V/Si devices with record dual-junction (GaAs//Si) and triple junction (GaInP/GaAs//Si) one-sun efficiencies of 32.8% and 35.9%, respectively [41]. The design flexibility afforded by 4T devices enables the use of subcell combinations that are not as sensitive to the material bandgaps, because current matching is not required. We then developed a novel 3T device geometry, which maintains design flexibility while eliminating the need for intermediate grids for electrical transport. We used rigorous device physics modeling to show that 3T devices can achieve efficiencies as high as 4T devices, and demonstrated an initial 27.3% efficient 3T device [11]. To accomplish this, we developed a transparent conductive adhesive (TCA) [42] which enables bonding of textured subcells in both 3T and 2T

configurations. Although these device designs can be applied to many subcell combinations, our initial works focused on III-V/III-V and III-V/Si platforms to demonstrate the concept, and to provide extremely high efficiency devices appropriate for high-value entry markets.

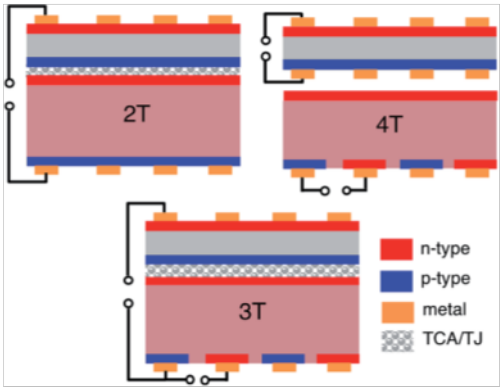

Figure 2 Schematics comparing wiring and interconnections for tandem solar cells operated in 2T, 4T, and 3T modes [36].

6. Project Objectives:

We focused our research to build upon prior results to develop optimized, >35% efficient III-V/Si multijunction solar cells interconnected via our low-cost TCA. This allows us to integrate industry-standard, textured Si solar cells with high efficiency III-V top cells. The simple III-V top cell structures are thin and compatible with low-cost growth techniques and substrate recycling technologies. The resulting bonded cells would achieve efficiencies rivaling optimized all-III-V multijunctions, but at costs compatible with non-concentrator applications. We investigated string and module level concerns as well, designing and demonstrating interconnection schemes for devices with different configurations, to understand the trade-offs and provide information about which device types are most appropriate for different applications. We also performed some outdoor testing and reliability experiments to understand how stacked tandems respond to likely environmental stresses, including for space PV conditions, which is a likely entry market for these high efficiency cells. This project was structured around three interrelated tasks:

Task 1. Fabricate prototype high-efficiency tandem solar cells.
To demonstrate the potential for high efficiency devices, it is critical to fabricate prototype devices at reasonable areas. This task focused on solar cell development.

Task 2. Application-Driven Tandem Device Design
A key part of this work was to understand the design guidelines for high-efficiency solar cells in prospective entry markets. We had previously created a rigorous device model for one incarnation of 3T tandems: a recombination-junction-interconnected GaInP/Si solar cell. These simulations show that this design is capable of efficiencies equaling 4T cells and exceeding 2T cells, and the *JV* results agree qualitatively with

as-yet-unoptimized experimental devices. We investigated both individual device configurations and strings in this task.

Task 3. Test the performance of tandem module components under realistic operating conditions.

Both silicon and III-V devices have excellent demonstrated reliability, meaning that the devices fabricated here can be expected to meet SunShot 2030 reliability targets. However, both terrestrial applications that require higher energy density (e.g. rooftops) and space PV have harsher operating environments than standard utility solar installations due to thermal cycling, radiation, etc. There are also potential differences in degradation mechanisms in tandems, where cells are exposed to different spectra than single junction modules. In this task, the impact of these conditions was be measured, and we worked to identify potential weak points that need to be further studied for long term reliability and performance. Two subtasks related to this are:

Subtask 3.1: Thermal cycling of TCA

The TCA material presents the largest unknown for the performance and reliability of the mechanically-stacked cells which will be produced in this project. Its performance has been thoroughly demonstrated in test structures as well as initial solar cells, including a prototype GaInP/Si dual junction solar cell with efficiency > 27%. This project, however, was the first investigation of TCA performance for large area solar cells and under stress-testing conditions. Our work evaluated the readiness of the TCA by using it in modules (via our industry partners) to demonstrate compatibility with commercial equipment. Critical functions that were assessed include transparency, resistance, oxidation resistance, mechanical creep, chemical inertness, degradation, etc.

Subtask 3.2: Design & fabricate a baseline device and test protocol

To identify weak points and enable device design improvements, we fabricated a baseline device, which was tested periodically over the project period to provide long-term data.

Table 1 (below) lists the project milestones, and the remainder of this report describes the results associated with these milestones.

Table 1. Project Milestones from TWP

Milestone	Description	Completed
1.1.1	Provide a detailed comparison of the performance of GaAs/Si 4T tandem solar cells growth by HVPE and MOCVD.	12/31/18
1.1.2	Fabricate three terminal, dual junction, III-V/Si bonded tandems using the TCA with efficiency > 30%.	
1.1.3	**Demonstrate that components can be scaled to larger areas (4cm2) while maintaining efficiency of >30%.**	**12/30/20**
1.2.1	Improve cell and string level models that enable comparison between different subcell configurations at a string level	7/9/19
1.2.2	Fabricate prototype strings containing at least 4 tandem devices and show that model and experiments agree with each other within 10% relative error (power output)	10/6/20

Milestone	Description	Completed
1.3.1	Test thermal cycling of TCA	6/30/19
1.3.2	Fabricate a baseline mechanically stacked tandem device and begin long-term outdoor testing.	10/22/19
2.1.1	Fabricate scaled up (4cm2) tandems with efficiencies >30%	
2.2.1	Develop taxonomy for 3T devices that enables compact circuit notation and develop analytical model to explain unique behavior from simple diode equations	3/31/20
2.2.2	Develop and verify procedure to extract equivalent circuit model components from uIBC and bIBC 3T devices	
2.2.3	**Fabricate strings of 3T cells**	**7/18/20**
2.3.1	Advanced reliability testing of TCA	10/31/20
2.3.2	Prepare packaged 3T cell for outdoor testing	
3.1.1	Fabricate 8-cell 3T strings	7/18/20
3.2.1	Update 3T string model to enable calculation of energy yield for strings using III-V/Si configurations.	9/30/21
3.2.2	**Predict the energy yield of strings**	**8/25/22**
3.3.1	Demonstrate IEC 61215 compatible packaging	

Project Results and Discussion:

3T Tandem Solar Cell Taxonomy

Since their initial introduction in the mid 1980s [37,43,44], 3T tandems have been left relatively uninvestigated until recently. Most III-V multijunction devices studied in the intervening years have utilized tunnel junctions [45,46] and adjustable III-V bandgaps for simple-to-use 2T tandem structures. Recent interest in developing hybrid tandems between Si and high-quality top cells such as III-V [35,39] or perovskites [34] has led to a rediscovery of the 3T tandem concept. The development of efficient and economical IBC Si bottom cells brought excitement for many hybrid 4T and 3T tandem concepts. The introduction of TCA as a glue to couple significantly different materials together also appeared enabling for hybrid 2T and 3T tandem structures. But at the beginning of this project many practical questions still remained about 3T operation, characterization, and utilization within a module.

These questions were systematically investigated within this project. We began the project by bringing the community together by publishing a standard taxonomy of 3T tandems [12] that catalogued the types of 3T tandems as shown in Fig. 3, and unambiguously labeled the three terminals and measurement configurations as shown in Fig. 4. This foundational publication satisfied Milestone 2.2.1 and laid the groundwork for further 3T tandem research. We used Sentaurus TCAD to simulate the performance of both uIBC and bIBC devices, confirming (without the use of any equivalent circuit models) that a 3T devices can operate in all the configurations shown in Fig. 3.

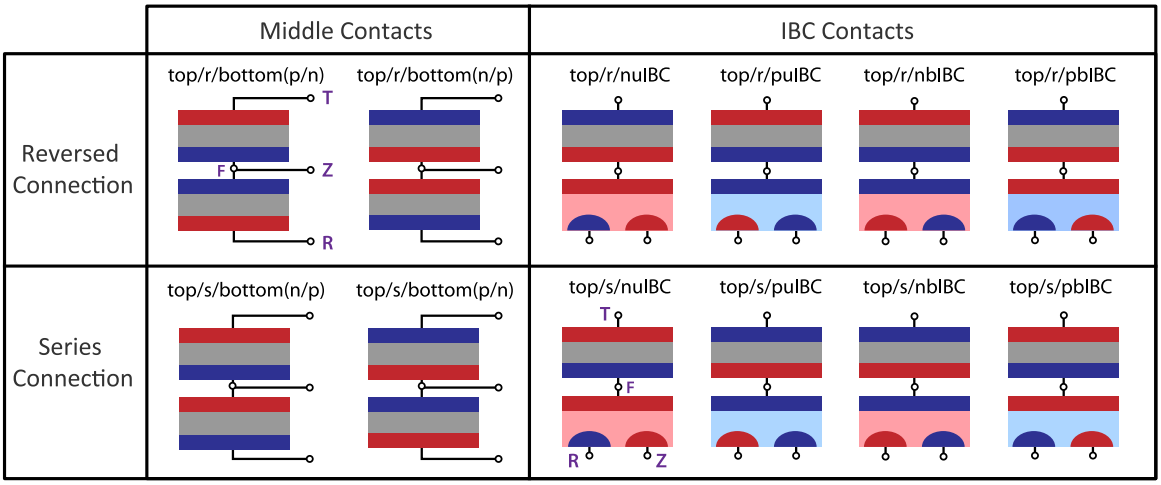

Figure 3. Schematics and standardized nomenclature for the wide variety of possible 3T tandems. N-type materials are red and p-type materials are blue.

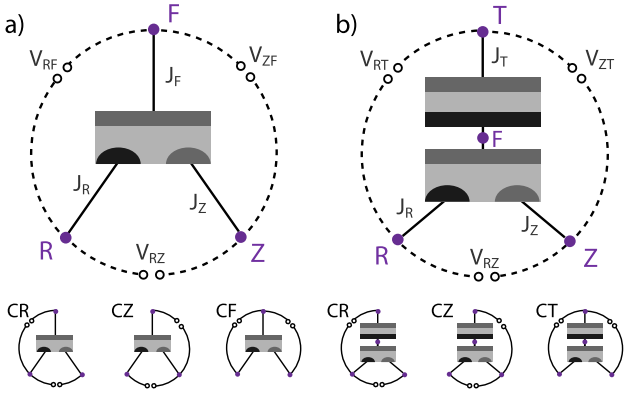

Figure 4. Node name and measurement-configuration conventions for (a) a standalone 3T IBC subcell and (b) a generic s-connected 3TT device. The node names are independent of the cell doping, so neutral colors are used. Each cell can be loaded in three different ways, indicated by which contact is common between the loads (CR, CZ, C(F/T)) as shown schematically below the larger diagrams.

4T III-V/Si IBC Tandem Cells

We have previously demonstrated high efficiencies with 4T III-V/gridded-Si [41] and III-V/IBC-Si [47] tandem solar cells as shown in the first four lines of Table 2, but the fabrication of the III-V subcells is currently cost-prohibitive for flat-plate, terrestrial applications due to the high costs of 1) MOVPE growth processes, 2) single-crystal III-V and Ge substrates, and 3) lithographic metallization processes. Other SETO-funded projects are targeting the reduction of these costs through substrate reuse by spalling and epilayer growth by a potentially cheaper process called Hydride Vapor Phase Epitaxy (HVPE). In this project we investigated the efficacy of using HVPE-grown top subcells compared to MOVPE-grown subcells as shown in Fig. 5. We demonstrated 4T GaAs//Si IBC tandems with over 29% efficiency using both MOVPE and HVPE-grown top cells [5], fulfilling Milestone 1.1.1.

Table 2. Novel 3T and 4T tandem structures fabricated at NREL

Structure	Efficiency	Publication
4T GaInP/glass/grided Si	32.5%	Essig 2017
4T GaAs/glass/grided Si	32.8%	Essig 2017
4T GaInP/GaAs/glass/grided Si	35.9%	Essig 2017
4T GaInP/glass/Si IBC	30.3%	Schnabel 2018
4T GaAs/glass/Si IBC (MOCVD)	29.6%	VanSant 2019
4T GaAs/glass/Si IBC (HVPE)	29.0%	VanSant 2019
4T GaAs/glass/Si IBC (vary t)	32.5%	Whitehead 2020
3T GaInP/TCA/Si IBC (substrate)	27.3%	Schnabel 2020
3T GaInP/TCA/Si IBC (superstrate)	21.3%	VanSant 2022
3T GaAs/TCA/Si IBC (superstrate)	21.3%	VanSant 2022
3T GaInP/s/GaAs (8 cells)	26.1%	Geisz 2020
3T GaInP/r/GaAs (8 cells)	27.8%	Geisz 2020

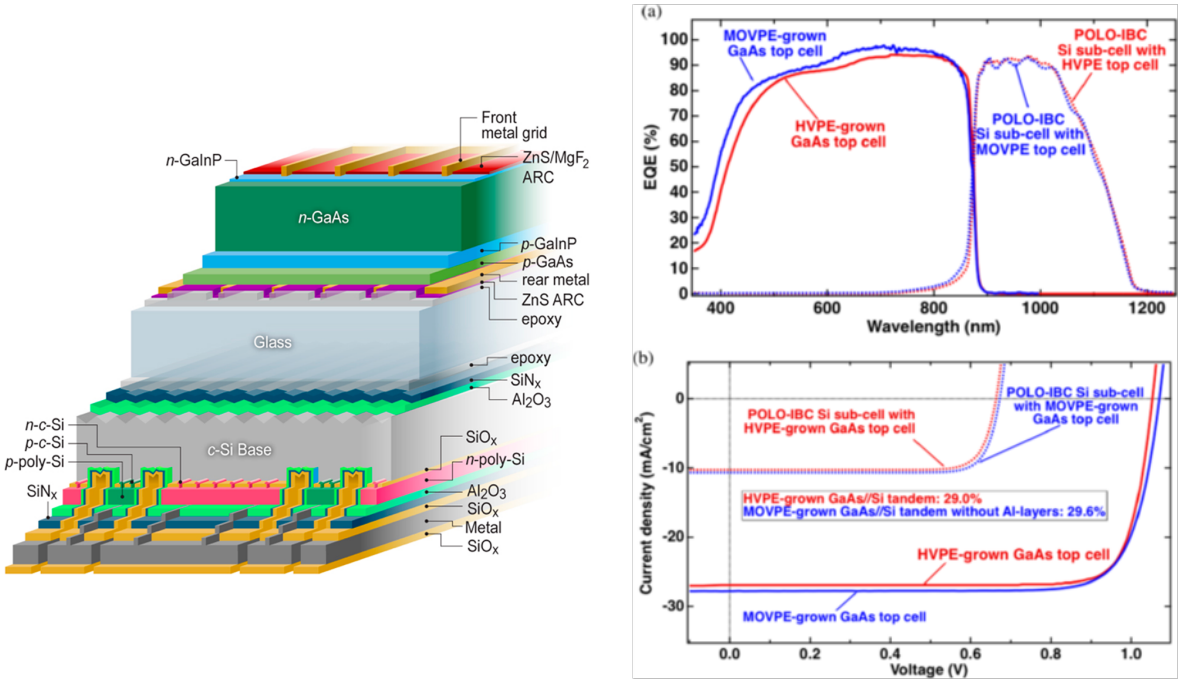

Figure 5. (left) Schematic of a 4T GaAs/glass/Si IBC solar cell. (right) Performance comparison between 4T tandem cells grown by MOVPE and lower cost HVPE processes.

To demonstrate that tandems using Si and III-V subcells are robust and reliable for long-term operation, 1-cm^2 4T MOCVD-grown GaAs//Si IBC tandems were packaged between glass by lamination with EVA sheets and silicon edge-seal encapsulants as shown outdoors in Fig. 6. These devices were measured continuously outdoors for over 100 days, fulfilling Milestone 1.3.2. They maintained a constant combined efficiency of 28% over this time with no significant degradation observed.

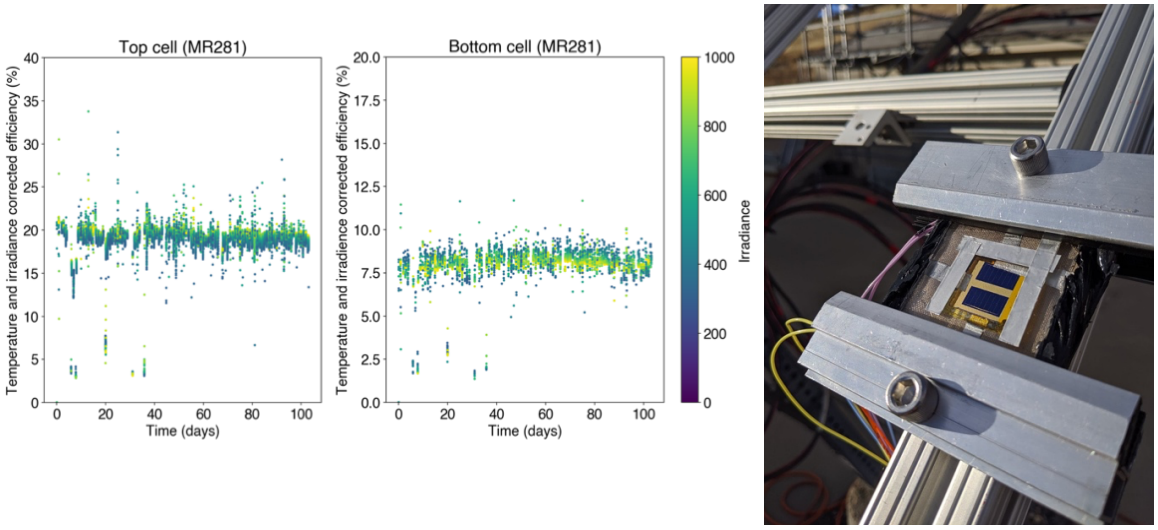

Figure 6. Corrected outdoor efficiencies of top and bottom subcells for a 4T GaAs/glass/Si IBC cell mounted outdoors (as pictured on the right).

Large area (4 cm^2) 4T tandems were also fabricated using GaAs epi from partner SolAero and Si IBC cells from partner ISFH (Fig. 7). Before lamination, these components reached a combined efficiency of 30.1%, fulfilling Milestone 1.1.3, but afterward dropped to 27.8% due to grid shading. COVID-related staffing issues unfortunately interrupted the continuation of this study. These results narrowly missed Milestone 2.1.1 because 30% efficiency was not demonstrated in the stacked device. These results show that these large area 4T devices can indeed be fabricated with high efficiency.

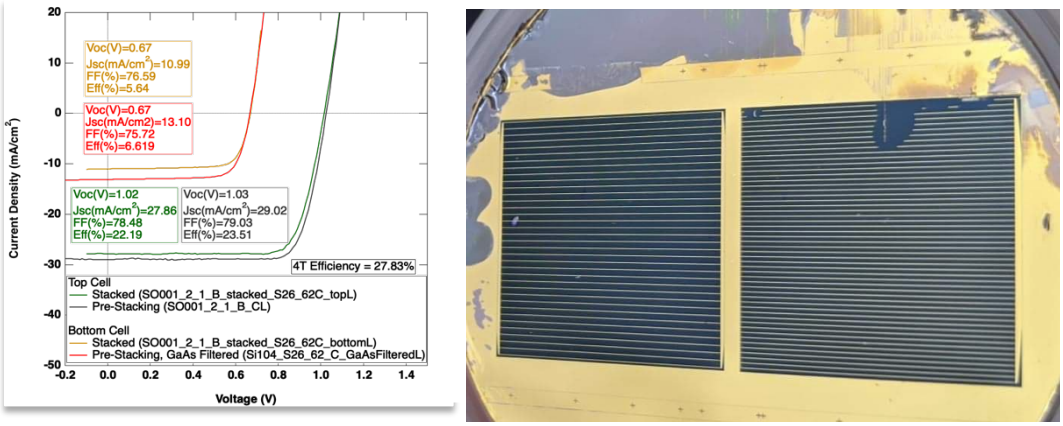

Figure 7. (left) Subcell JV curves of large area (4 cm^2) 4T GaAs/glass/Si IBC tandem solar cells. (right) Photo of two 4 cm^2 GaAs subcells processed on a 4 inch wafer grown at SolAero.

Optimization of the 4T GaAs//Si tandem was also investigated by varying the thickness of the GaAs top subcell [22]. This study revealed that high-index (e.g. glass) dielectric interlayers in 4T tandems have the added benefit of significantly reflecting emitted light from the top subcell resulting in photon recycling. Surprisingly, this device

structure was relatively insensitive to the thickness of the top GaAs subcell. The high top-cell-Voc and Jsc results of the study can only be explained by photon-recycling-enhanced voltages and diffusion lengths.

3T Si IBC cells

Three-terminal Si IBC cells for this tandem project were developed at ISFH in cooperation with our team at NREL [2]. A lean PERC process [3] for the fabrication of IBC solar cells was developed at ISFH as shown in Fig. 8. These 3T Si IBC solar cells were used as the basis of our hybrid tandem solar cells at NREL.

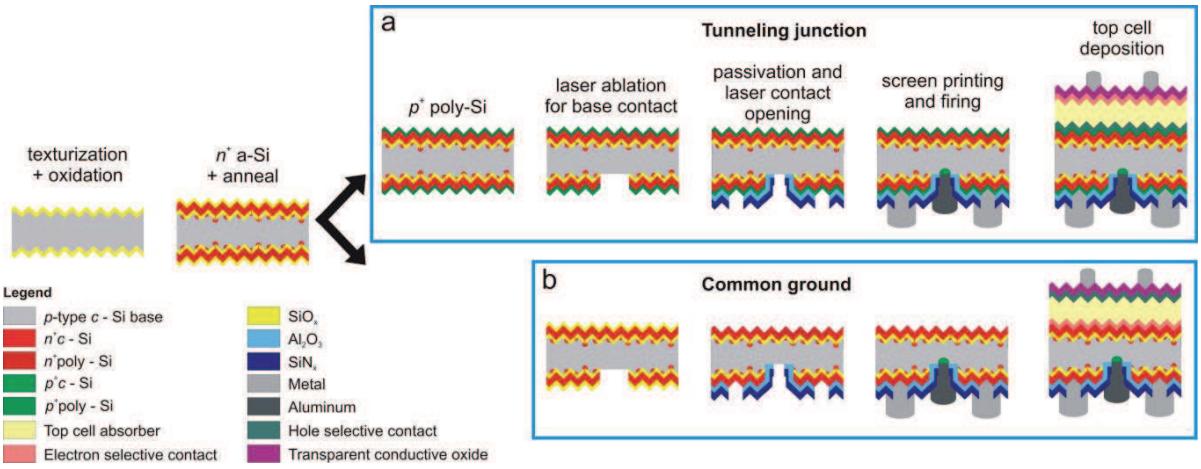

Figure 8. Simplified Si IBC fabrication process for (a) a tunnelling junction type and (b) a common ground type 3T tandem featuring a bipolar junction bottom cell.

Two types of 3T Si IBC were identified within the taxonomy as 1) unipolar (uIBC), with a single emitter (p-n junction) at the back (R) contact and 2) bipolar (bIBC), with a minority-carrier selective contact at both the front (F) contact and the additional (Z) contact as shown in Fig. 9. In an IBC cell, the bottom-surface location of the extra (Z) contact enables injection or extraction of excess current (which eliminates the current-matching restrictions inherent to 2T tandems) without requiring an intermediate grid between the subcells. This can simplify design and fabrication and eliminates the electrical and optical-shadowing losses associated with an intermediate grid.

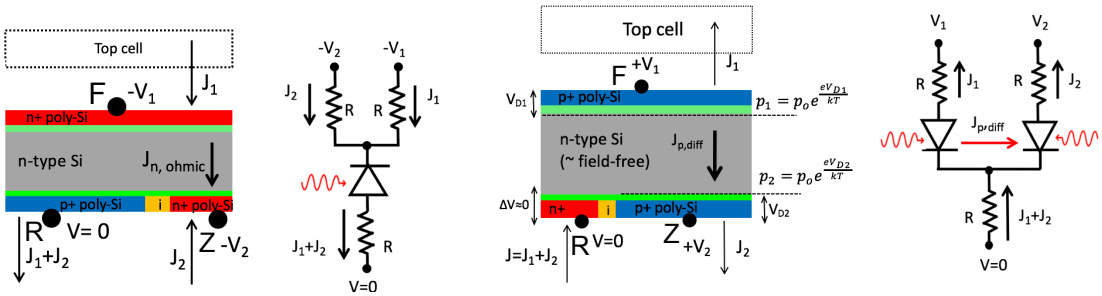

Figure 9. Schematics and equivalent circuit diagrams of 3T single-junction IBC solar cells: (left) unipolar IBC and (right) bipolar IBC.

We predicted the operation of these single-junction 3T Si IBCs with a simple physical model early in the project [4] as shown in Fig. 10A and 10B. Unipolar 3T IBC devices

from ISFH were later measured at NREL as shown in Fig. 10C and 10D, and fit using the *PVcircuit* software described later in this report. Excellent agreement between the prediction, measurements and fit were obtained. The publication of a more complete description of the equivalent-circuit for these 3T IBC devices was targeted in Milestone 2.2.2, but due to staffing limitations this work remains unpublished in a peer-reviewed journal.

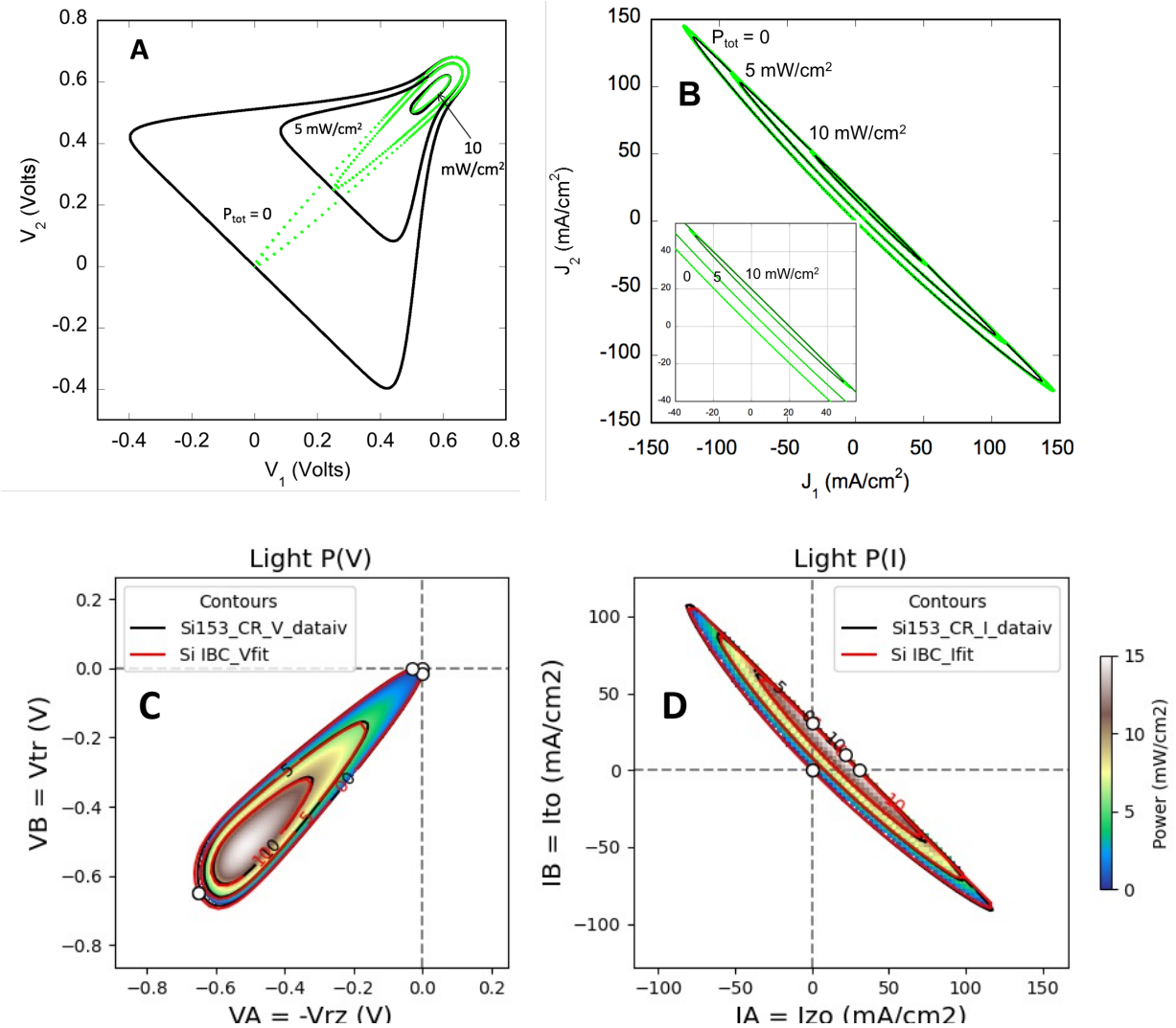

Figure 10. Predicted (A&B) and measured (C&D) operation of single-junction 3T IBC solar cells (A) Predicted power [4] as a function of voltages (PVV) plots of unipolar (green contours) and bipolar (black contours) IBC solar cells. (B) Predicted PJJ plots corresponding to A. (C) Measured (black contour and color) PVV plots of unipolar (nuIBC) solar cell from ISFH fit (red contour) to an equivalent circuit with *PVcircuit* software. (D) Measured and fit PJJ plots corresponding to C.

Transparent Conductive Adhesives (TCA)

This project used a TCA composed of a polymer−particle blend with ethylene-vinyl acetate (EVA) as the transparent adhesive, and metal-coated flexible poly(methyl methacrylate) (PMMA) microspheres as the conductive particles to provide conductivity and adhesion regardless of the surface texture as shown in Fig. 11. This

TCA layer was designed to be nearly transparent, conductive in only the out-of-plane direction, and of practical adhesive strength to hold the substrates together [42].

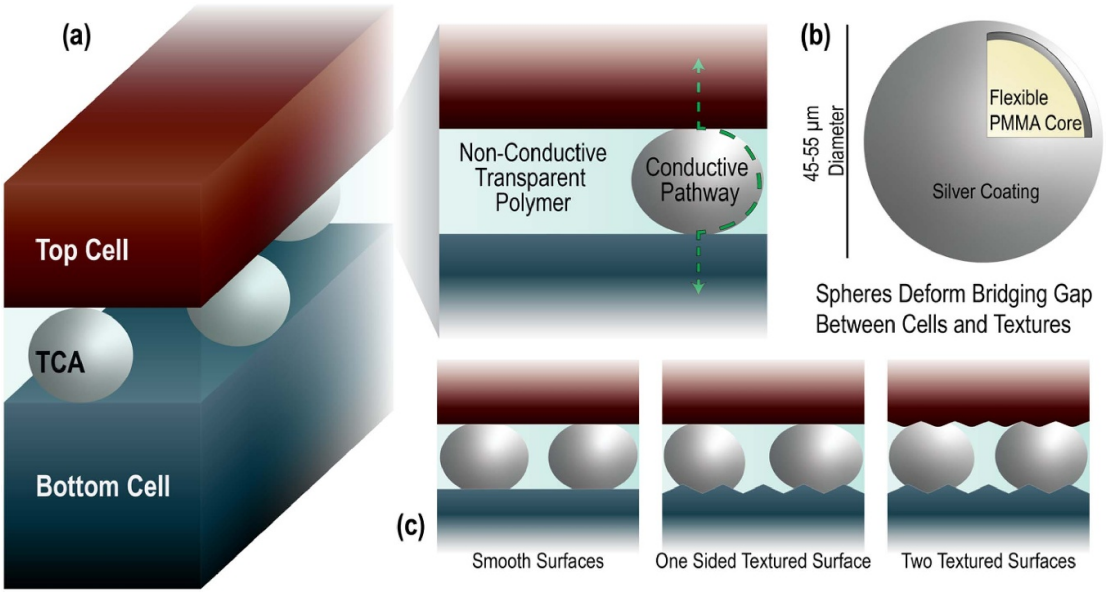

Figure 11. (a)Transparent conductive adhesive (TCA) shown within a tandem solar cell stack, as a single layer of conductive microspheres (45–55 µm in diameter), held together with a transparent non-conductive polymer. (b) The compliant microspheres have a flexible PMMA core with a silver coating (c) allowing the spheres to electrically connect both smooth and textured surfaces with micron sized surface features.

TCA sheets fabricated by blade coating, similar to EVA encapsulant sheets, were developed for lamination of dissimilar subcells to enable hybrid tandems [19]. Particle coverage and lamination process parameters are important for optimizing series resistance and optical transparency within tandems. To address Milestone 2.3.1, we studied the reliability of TCA interconnects with thermal cycling (IEC 61215.10.11 : TC100) and damp heat (IEC 61215.10.13 : DH1000) testing protocols on custom designed TCA test coupons with edge card reader connections (Fig. 12).

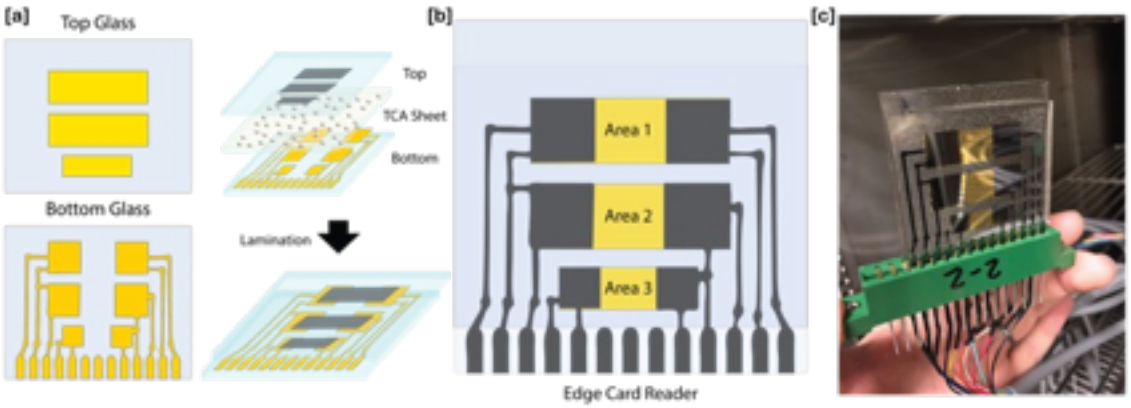

Figure 12. [a] Sample design of the TCA test coupons for thermal cycling and damp heat testing. [b] Schematic of TCA alignment and edge-card-reader connections. [c] Sample installed in one of the edge-card-readers within the chamber.

In our initial testing, the average series resistance of optimized samples was within 25% of the initial resistance value. However, it was observed that at temperatures above 80°C, the original TCA formulation (which did not have any additives) softened enough to cause top glass to slide out of alignment with for the measurement. During this softening stage, the TCA was still vertically conductive – contact was simply lost when samples moved enough that there was no longer vertical alignment of the contact pads.

An improved TCA formulation using additives was then fabricated and went through IEC 61215 damp heat and thermal cycle testing. The addition of surface primers and crosslinking agents improved the performance of the TCA in these reliability tests (Fig. 13). The series resistance of the samples actually improved, decreasing by 19% over 1000 hours of damp heat.

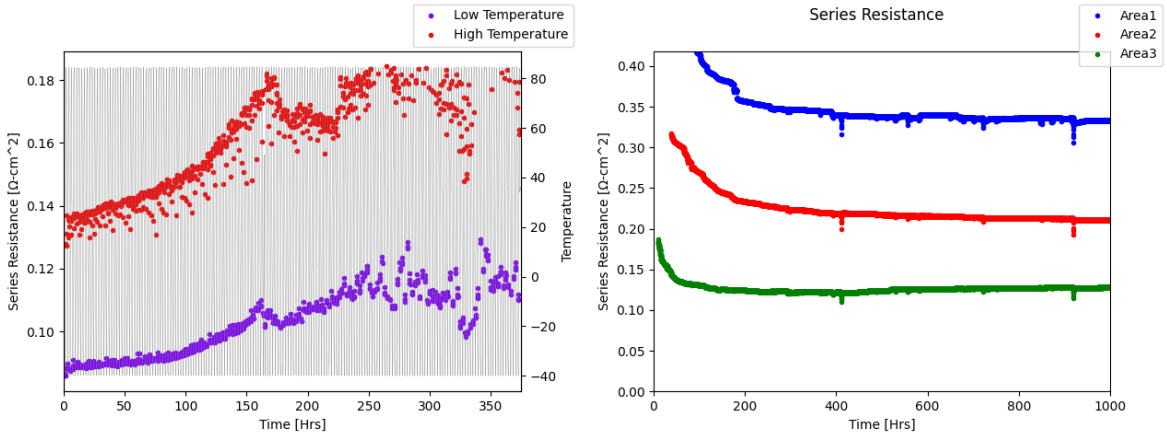

Fig 13. (left) Series resistance of TCA measured at both 85°C and -40°C over 100 thermal cycles. At room temperature, the final resistance increased by 18% after the test. (right) Series resistance of TCA measured over 1000 hours of damp heat testing (85/85).

3T III-V/TCA/Si IBC cells

After our previous successful demonstration of high-efficiency 4T tandems with III-V on Si [41] and demonstration of the equivalence with 3T tandems [47], we began to work on the practical aspects of developing III-V/TCA/Si IBC cells. We demonstrated the first 3T tandem with TCA [11] by processing an inverted GaInP top cell stacked directly onto a Si IBC cell as shown in Fig. 14(a). This 3T tandem achieved an efficiency of 27.3% as shown in Fig. 14(b), but this process flow appeared tenuous because it exposes the completed Si bottom cell to possible damage during top subcell processing.

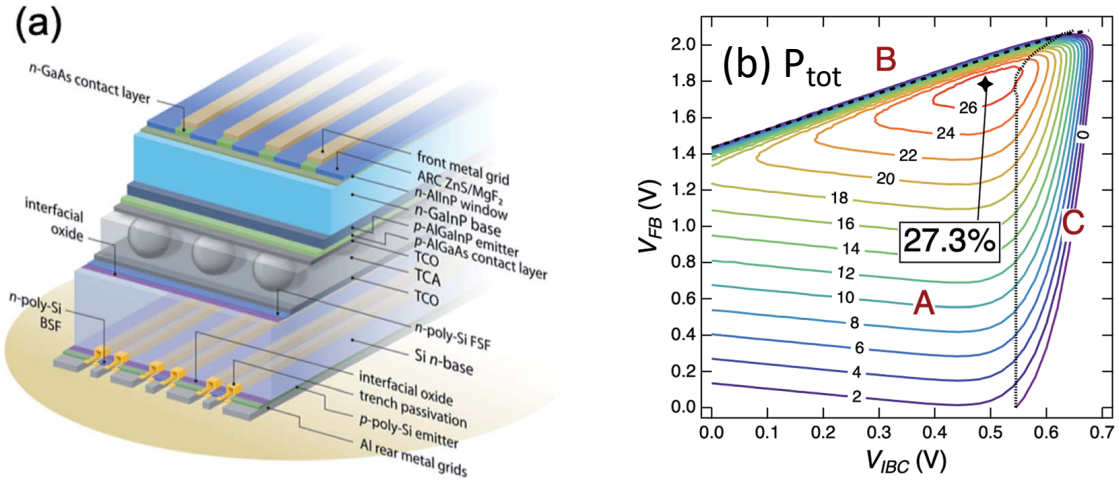

Figure 14. (a) Schematic of a 3T GaInP/TCA/Si IBC tandem fabricated by processing an inverted GaInP cell directly onto a Si IBC subcell. (b) Contour plots showing the measured total power of the 3T tandem under AM1.5G illumination.

For a more robust process flow, we envisioned [21] separately processing an upright III-V subcell onto superstrate glass, then lamination of the two completed subcells with a TCA sheet. These 3T superstrate GaInP/TCA/Si IBC and GaAs/TCA/Si IBC tandem solar cells, shown schematically in Fig. 15, were fabricated [26] using ISFH Si IBC bottom subcells. Measurements of these 3T tandems are shown in Fig. 16. The unconstrained maximum of each device was 21.3% - 22.3% efficiency, depending on the measurement technique. When constrained to have equal currents through both subcells as in a 2T tandem, the tandems were 20.8% and 12.1% efficiency respectively. These results clearly demonstrate the design flexibility of 3T over 2T tandem structures.

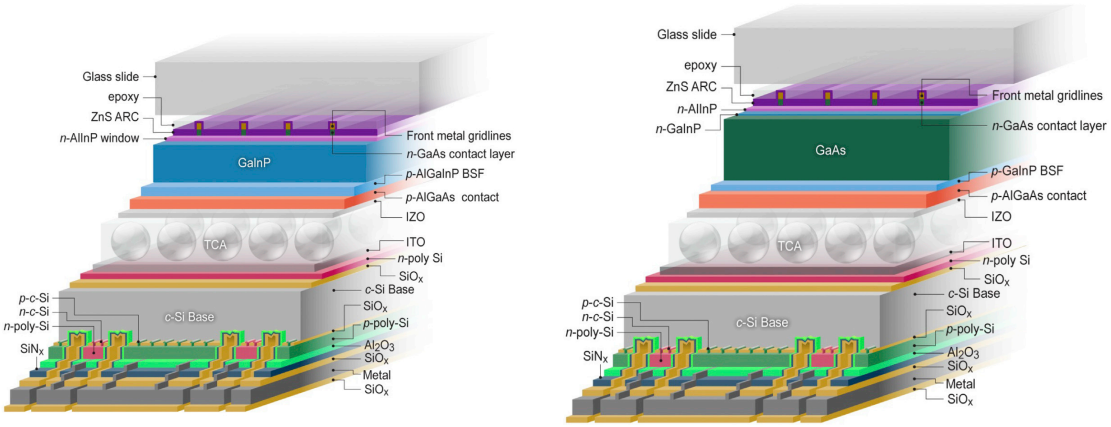

Figure 15. Schematics of superstrate 3T tandem solar cells: (left) a GaInP/TCA/Si IBC tandem cell and (right) a GaAs/TCA/Si IBC tandem cell.

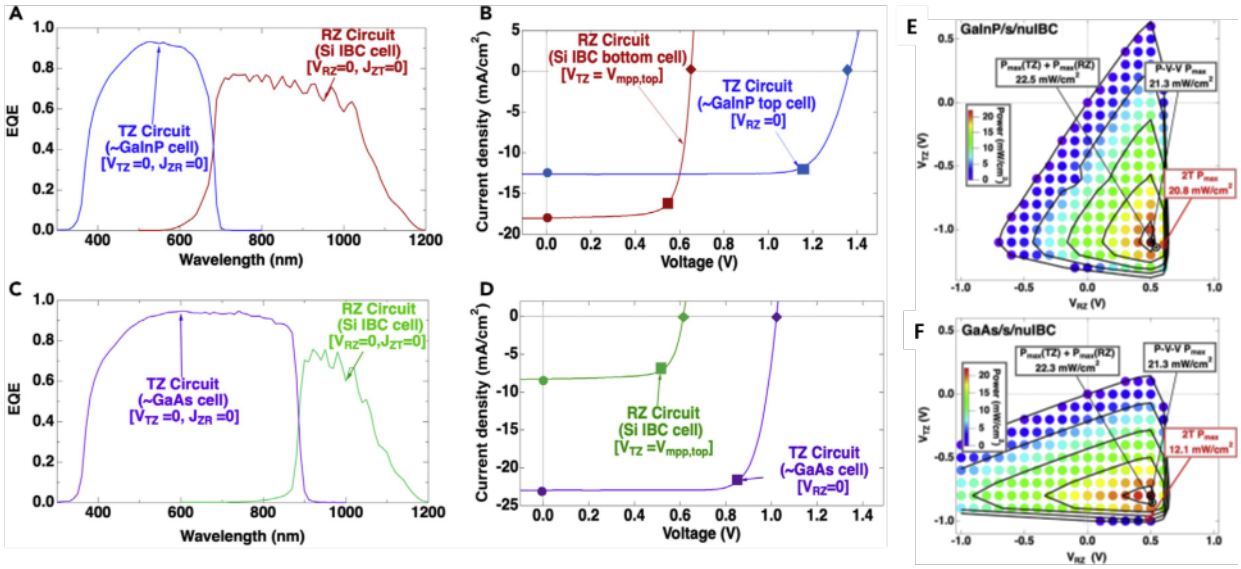

Figure 16. Measured results of (A,B,E) GaInP/TCA/Si IBC and (C,D,F) GaAs/TCA/Si IBC hybrid 3T tandems. (A&C) show subcell EQE results. (B&C) show subcell JV curves with the other subcell held at a constant voltage as indicated. (E&F) show coupled power as a function of subcell voltage (PVV) plots at AM1.5G illumination.

Unfortunately, this relatively low efficiency included several losses such as the lack of antireflective coating on the top glass, resistive losses from the TCO contact layers and TCA interconnection, parasitic optical absorption, etc., that prevented surpassing the 30% efficiency required in Milestone 1.1.2. This TCA lamination process was plagued with problems of cracking glass and Si IBC cells, shorting layers, and irreproducible TCA resistance that resulted in low device yields. The specific working devices shown here contained III-V subcells that performed worse than similar subcells previously demonstrated, and the devices could not be replicated due to the low yields and COVID-related staffing issues. Many of these problems were addressed by redesigning the III-V mask to avoid potential shorting from metal overlapping, using thicker superstrate glass, and precisely laser scribing the Si IBC cell during the no cost time extension (NCTE) in order to fabricate an IEC 61215

compatible package as shown in Fig. 17. The cell results for glass-glass and glass-backsheet packages are shown in Fig. 18.

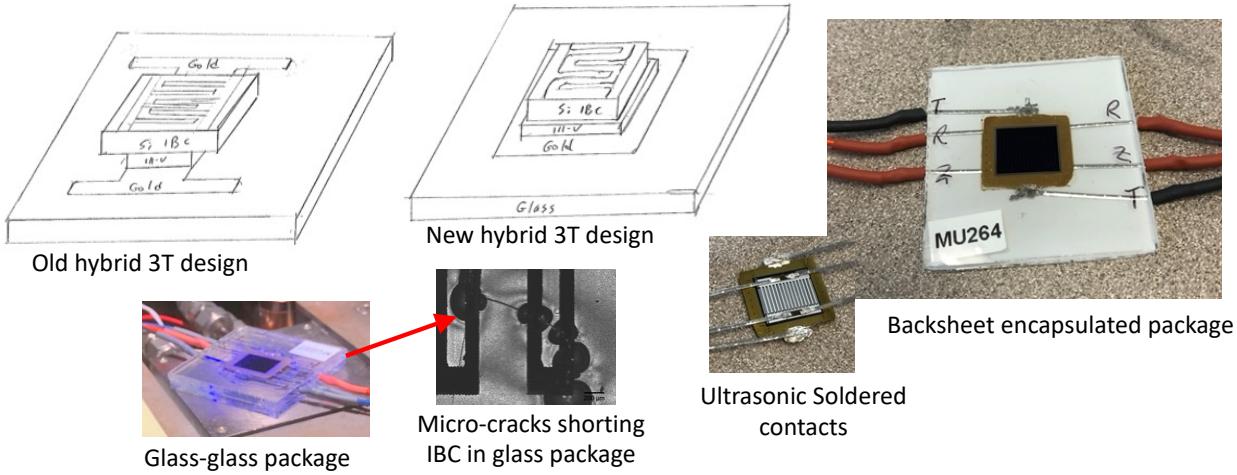

Figure 17. Redesigning 3T hybrid tandem packaging for IEC 61215 compatible measurements.

Though many problems were overcome with the redesign, high resistance to the top GaAs subcell ultimately prevented us from reaching the 20% efficiencies necessary as a starting point of the damp heat tests, therefore we were unable satisfy Milestones 3.3.1 and 2.3.2. This resistance is likely due to unoptimized TCA lamination conditions or high contact resistance between III-V and TCO layers and was particularly detrimental to the high-current GaAs subcell. Several lessons were learned during this process redesign that will be useful going forward for perovskite/Si tandem packaging.

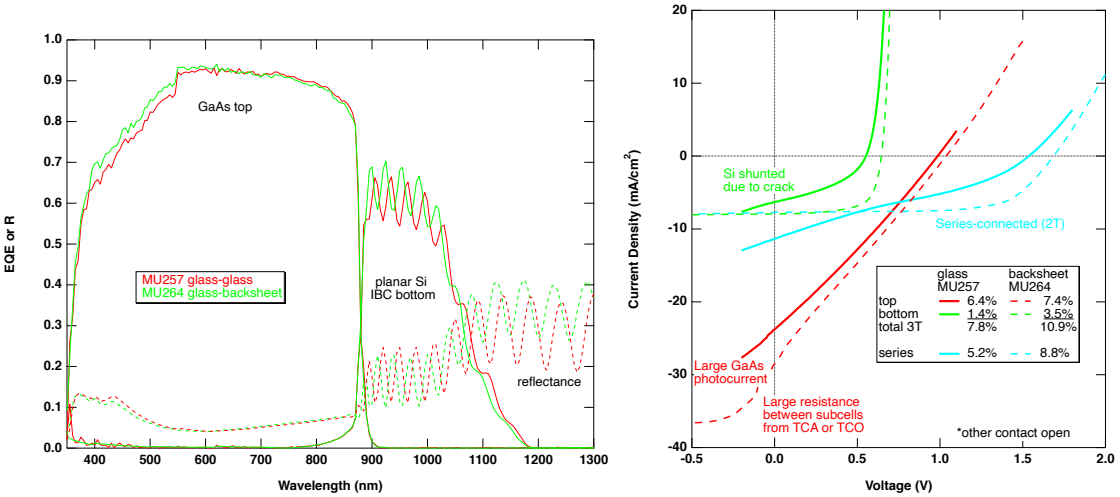

Figure 18. Measurements of the packaged superstrate 3T GaAs/TCA/Si IBC devices shown in Fig. 18. (left) EQE and (right) JV curves.

GaInP/GaAs 3T tandems

In order to make progress with understanding 3T tandem operation in spite of challenges in the 3T III-V/TCA/Si IBC process, we also developed all-III-V 3T tandems using stable, robust, inverted GaInP/GaAs tandem structures [7,17]. The process flow shown in Fig. 19 resulted in three external contacts supported by transparent flip-chip epoxy on a glass support holder pictured in Fig. 20 (left).

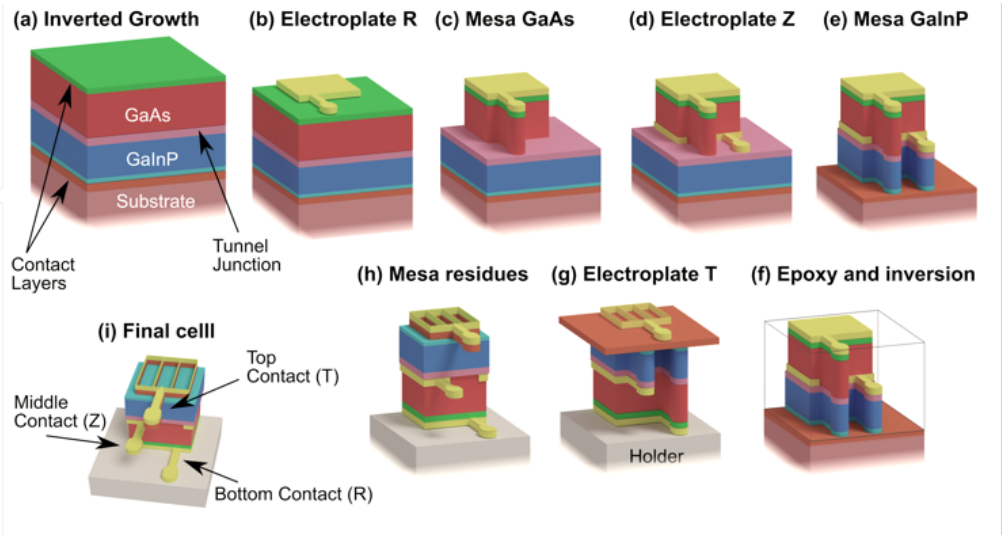

Figure 19. Process flow for fabrication of monolithic, inverted GaInP/GaAs 3T tandems with a middle (Z) perimeter contact. The top GaInP subcell is blue and the bottom GaAs subcell is red.

This process enabled the high-yield fabrication of eight 3T tandems with external contact pads on a single glass holder as shown in Fig. 20 (left) in both s-type and r-type configurations (depending on the epilayer design). There are many different ways these 3T can be interconnected to form a string; here we investigated "voltage-matched" strings in which the resulting module has two terminals such that it can be connected to a single load. In a voltage-matched string, the wiring topology constrains the cells to have a "voltage-matching" (VM) ratio defined to be V_{top}/V_{bot} = m/n, where m and n are integers. In principle, any ratio m/n is allowed, giving tremendous design flexibility. In practice, there are end losses associated with VM strings that favor small values of m and n. To enable the proper design of VM strings, we developed a general framework and end-loss model for stringing 3T tandems together into voltage-matched modules that explains the intrinsic end-losses [10,38,39]. An example for V_{top}/V_{bot} = 2/1 is shown in Fig 21 (left), using both s-type and r-type 3T tandems. From an analysis of breadboard diagrams like the one shown in Figure 21 (right), simple analytical expressions which inform string design were derived for the end losses of various string configurations.

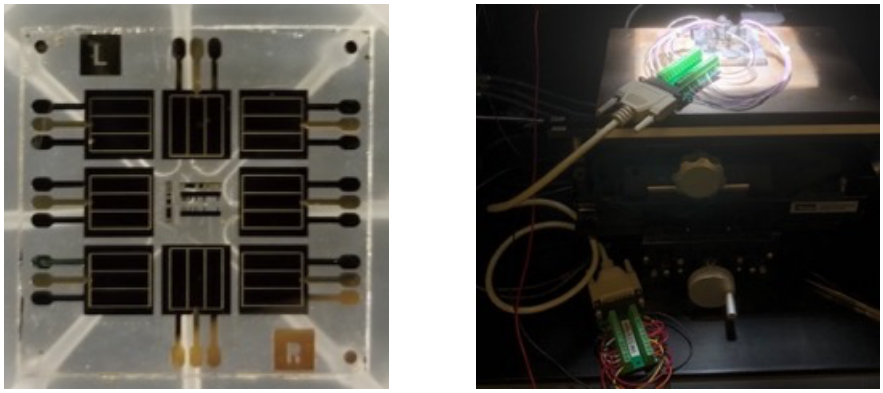

Figure 20. (left) Eight 3T GaInP/GaAs tandems with external contacts on a 1x1inch glass support. (right) 8-cell module of these cells interconnected using a multi-probe jig and external wiring module for 2:1 or 3:2 voltage-matched strings.

Using a contacting jig and external wiring to configure modules as shown in Fig. 20 (right), we demonstrated s-type and r-type, 2:1 and 3:2 voltage matched (VM) strings with 8 cells. The measured string results shown in Fig. 22 agree with model predictions, satisfying Milestones 1.2.2, 2.2.3 and 3.1.1.

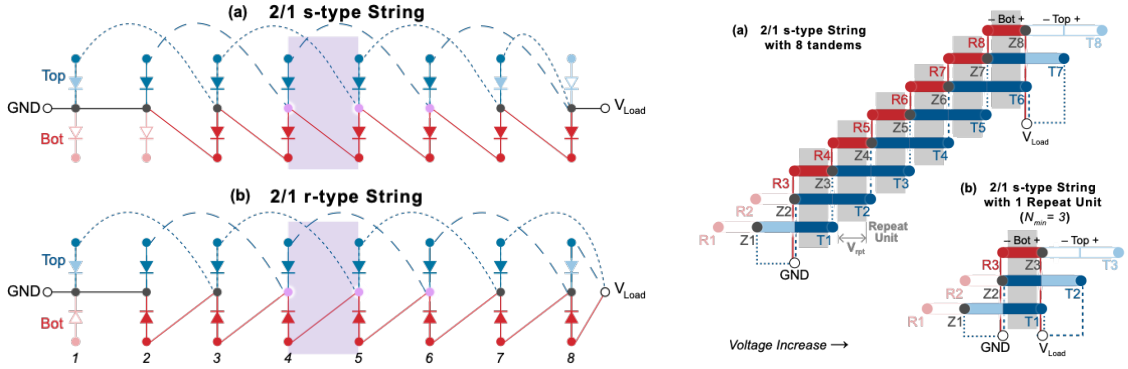

Figure 21. (left) Examples of VM strings using a VM ratio V_{top}/V_{bot} = 2/1 for (a) s-type and (b) r-type 3T tandem cells. The string can be made arbitrarily long by adding "repeat units" (purple box) to the middle of the string. However, the current paths are interlaced, so there are inherent string-end losses associated with how the ends of the strings must be configured to collect all of the current. To illustrate this, the subcells contributing to the end loss are shaded differently. Open cells are disconnected and produce no power. Lightly-shaded top cells produce $V_{top} = V_{bot}$ (instead of $2*V_{bot}$). (right) A "breadboard" circuit schematic helps with the understanding of these end losses. The example shown here is for an s-type 2:1 3T VM string. From these diagrams, it can be deduced that the end loss for this type of string is (approximately) $2*P_{tandem}$, where P_{tandem} is the power produced by each of the middle repeat units.

The string results shown in Fig. 22 illustrate the principal characteristics of our modeling: (1) End losses are smaller for r-type 3T cells (than for s-type), (2) end losses become larger as m and n become larger, and (3) increasing the string length reduces the impact of end losses. These findings inform the design and development of VM strings.

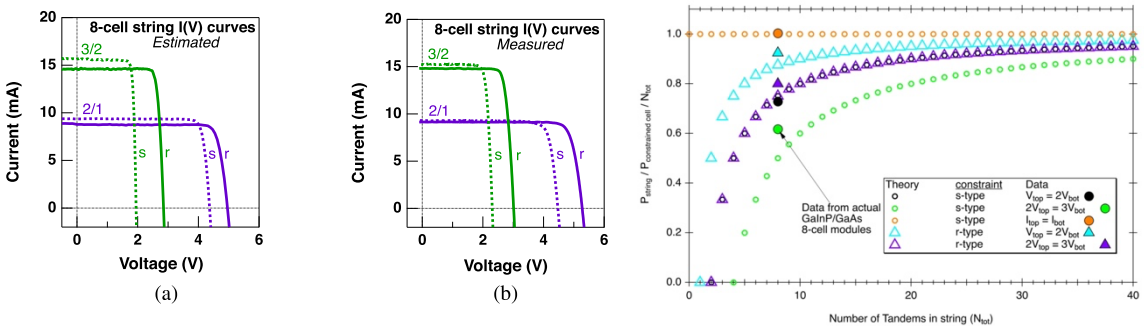

Figure 22. (left) Estimated IV curve of a voltage-matched string of 8 GaInP/GaAs 3T tandems. (middle) Measured IV curve of a voltage-matched string of 8 GaInP/GaAS 3T tandems. (right) Approximate end-loss trends as a function of string length and interconnection scheme. Small points show theory and large points show the data for the 8-cell modules.

Using these robust all-III-V 3T tandems as examples, we also developed a measurement platform and methodology [18] for all 3T tandems as shown in Fig. 23 (left). This methodology quantitatively explains the ambiguity of measuring 3T devices with two loads using the various common-contact modes as shown in Fig. 23 (right) and can characterize voltage-matched module operation with measurements of a single 3T tandem cell. Coupled dark J-V curve measurements (Fig. 24 (right)) are a sensitive technique to characterize both the electrical and optical subcell coupling in 3T and 4T devices.

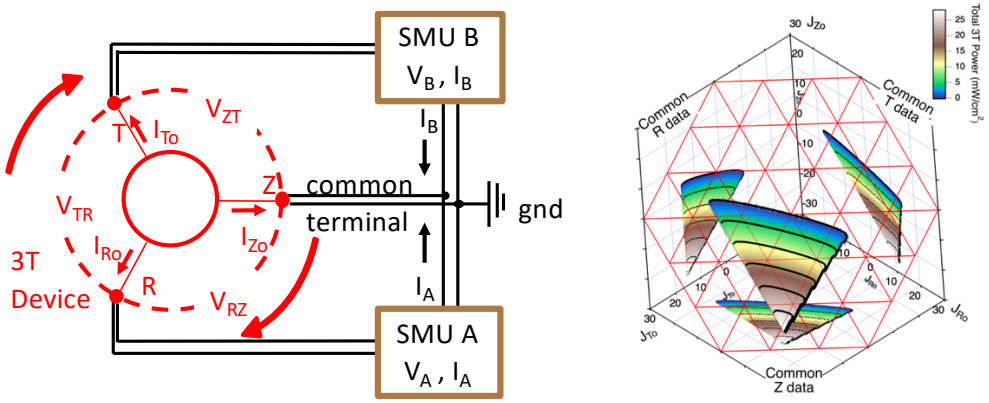

Figure 23. (left) Schematic of 3T and 4T measurement equipment. (right) Power as a function of three interdependent currents (PVVV) measured for an r-type 3T GaInP/GaAs solar cell in CZ, CR, and CT modes. The hexagonal representation of the data helps illustrate the equivalency of these different measurement modes (through Kirchhoff's laws).

The optoelectronic equivalent-circuit model shown in Fig. 24 (left) was also developed and included in the supplementary information of Ref. [18] to quantitatively explain the physics of electrical and optical subcell coupling in 3T and 4T tandems. The subcell coupling is the reason that the subcells should not be measured independently. The measurement and modeling of coupled dark JV curves in Fig. 24 (right) is so sensitive that even reverse luminescent coupling (LC) that is 6 orders of magnitude smaller than forward LC can be observed and fit. The modeling code is freely distributed, as requested by SETO, in an open-source, Python-based software package called *PVcircuit* [25,28].

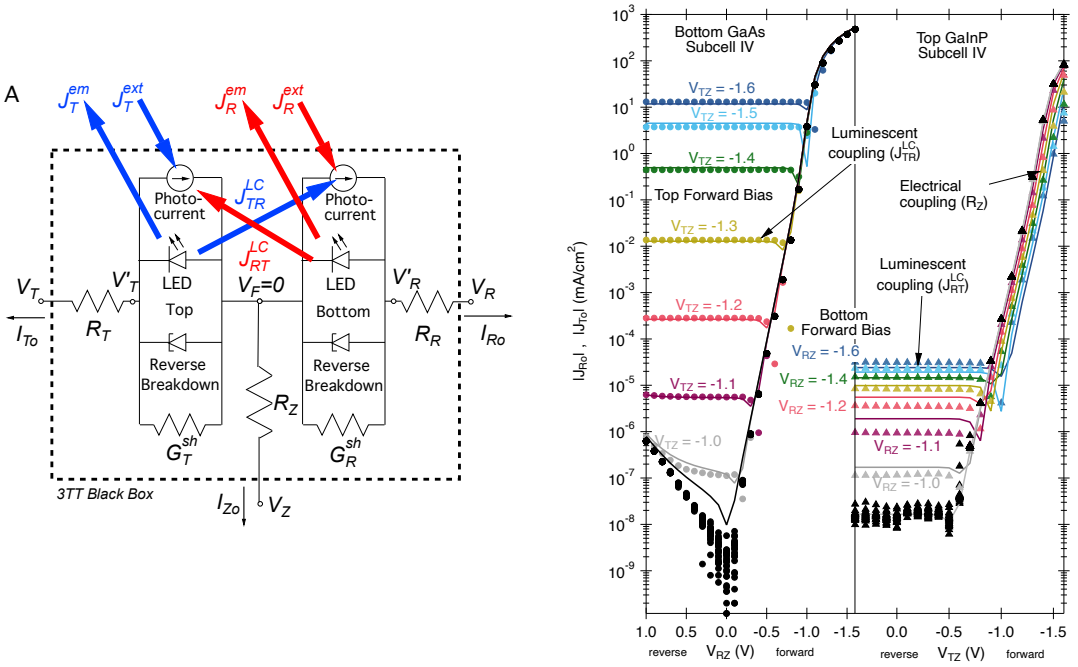

Figure 24. (left) Schematic of our 3T tandem optoelectronic equivalent-circuit model. (right) Coupled dark JV curves for an r-type 3T GaInP/GaAs solar cell.

Combining this model with proxy spectra produced by machine learning [48,49], we have performed energy harvesting efficiency (EHE) analysis [27] at a location in Boulder, CO satisfying Milestones 3.2.1 and 3.2.2. The EHE analysis process flow is summarized in Fig. 25, and the results are shown in Fig. 26. This EHE analysis is also incorporated into the *PVcircuit* software. The best terminal configuration is highly dependent on the bandgap combination of the tandem and the associated optical and resistive losses. 3T and 4T tandem designs open up possibilities for many new material combinations for hybrid tandems.

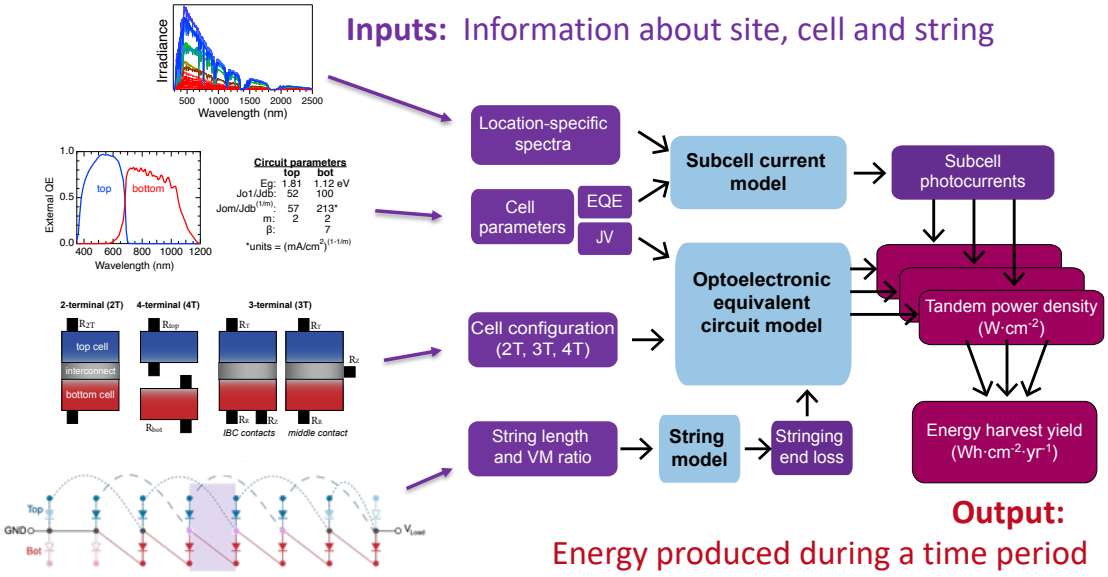

Figure 25. Process flow for EHE analysis.

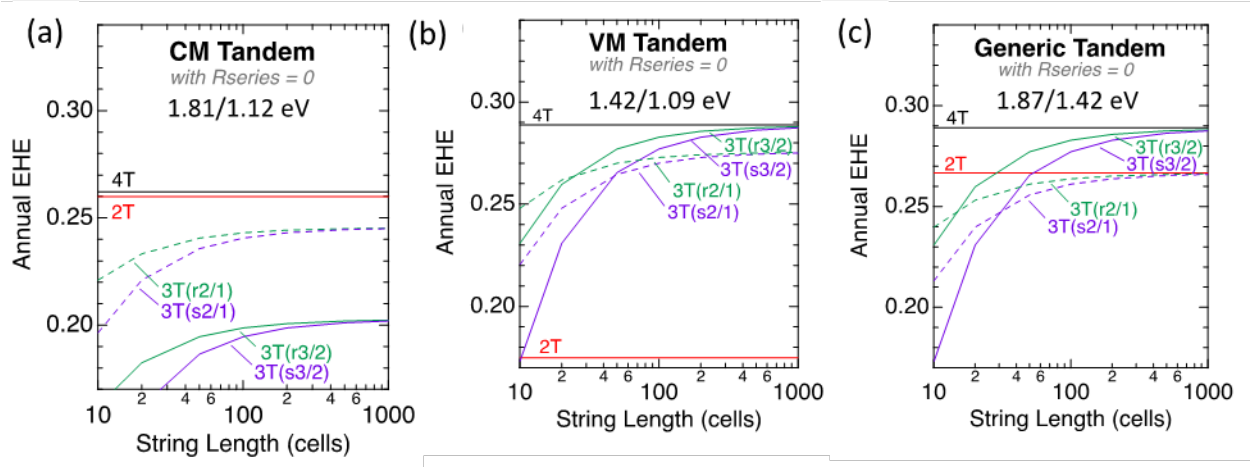

Figure 26. Comparison of EHE for various tandem-cell terminal configurations and interconnection schemes in Boulder, CO for three example tandem-cell designs: (a) Nearly current-matched tandem bandgaps 1.81 eV/ 1.12 eV. (b) Nearly voltage-matched tandem bandgaps 1.42 eV / 1.09 eV. (c) Intermediate generic bandgap combination 1.87 eV / 1.42 eV.

Quasi-random light-trapping texture

We have also investigated novel light trapping structures to improve the performance of ultra-thin III-V subcells, which in the future could become the top subcells for tandem cells. This work jointly funded with the III-V core project (Award DE-EE00034358) and is not associated with any milestones of this project. Quasi-random (QR) structures are predicted to have highly efficient light-trapping, while being more robust under angle and thickness variations than simple photonic crystals (Fig. 27) [1,8,15]. We have experimentally demonstrated a light-trapping solution based on QR photonic crystals fabricated by polymer-blend lithography [16,24]. We control the average lattice parameter by modifying the spin-coating speed to adjust the light trapping properties of the QR layer as shown in Fig. 28. We have demonstrated an ultrathin GaAs cell of 260 nm with a rear quasi-random pattern with submicron features [24], a Jsc = 26.4 mA/cm2 and an AM1.5G efficiency of 22.35%.

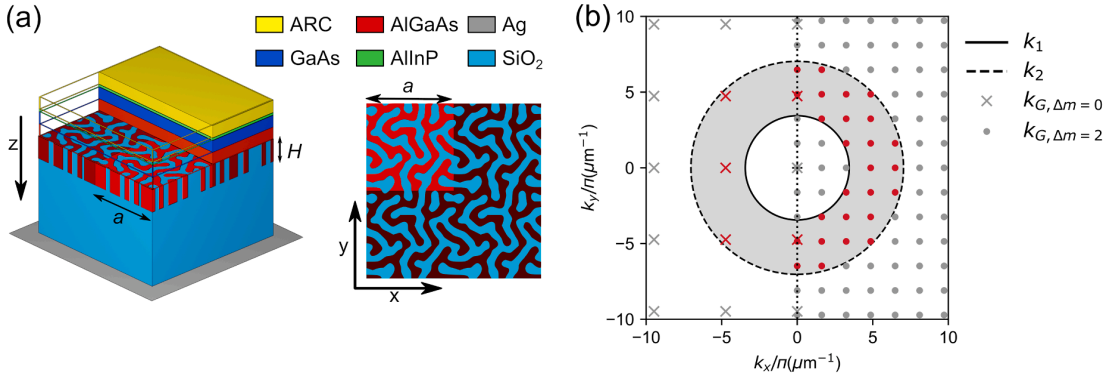

Figure 27. (a) Schematic of the layer structure of a thin solar cell incorporating QR texture at the back. The inset QR structure can be modeled with a repeat unit cell shown in red and can be fabricated with immiscible polymer blend lithography. (b) Reciprocal space representation of the QR pattern reveals a ring of spectral frequencies for a broadband photonic crystal that spans the solar spectral range.

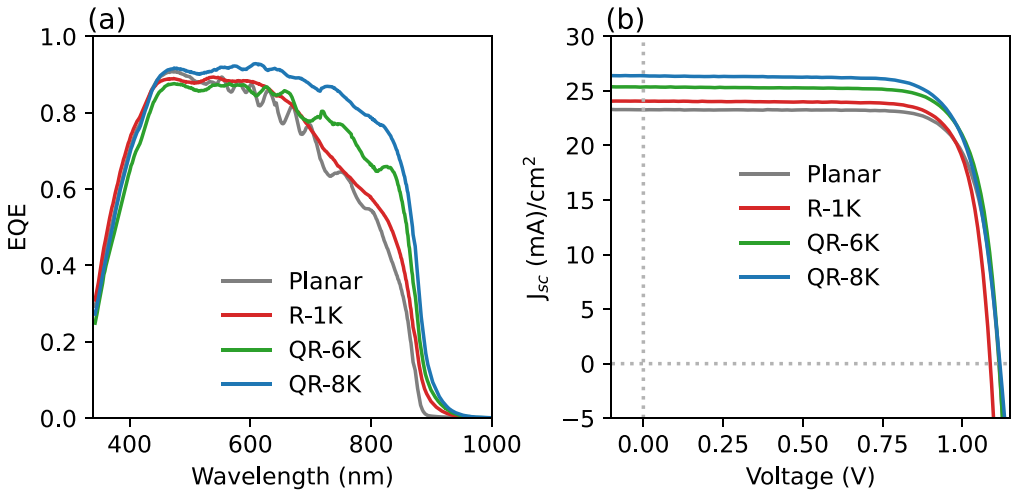

Figure 28. (a) EQE and (b) JV curves of an ultra-thin (260nm) GaAs-absorber solar cell, with various QR photonic back textures determined by spinner speeds for PMMA/PS polymer blend deposition: planar (grey), 1000 RPM (red), 6000 RPM (green), 8000 RPM (blue).

7. Significant Accomplishments and Conclusions:

This project proposed to fabricate high-efficiency prototype tandems (Task 1) with TCA and Si IBC bottom cells to understand the design guidelines (Task 2) and performance under realistic operating conditions (Task 3) for 2T, 3T, and 4T hybrid tandem solar cells. The challenges of developing a robust process flow for high-yield fabrication of hybrid tandems was formidable. Achieving the milestone target >30% efficiency for prototypes cells with large areas in robust packaging was therefore not accomplished due to these technical challenges and COVID-related staffing issues, but the general concepts were proven. Pivoting to demonstrations of robust all III-V cells allowed us to develop foundational knowledge of understanding, describing, measuring, modeling, and stringing 3T solar cells. This foundational knowledge is the most significant and lasting achievement of the project, as it has been clearly explained in peer-reviewed literature and open-source software for posterity.

8. Budget and Schedule:

The $3M budget was accurately spent within the 3.5 year schedule of the project with the addition of a 6 month no-cost technical extension. COVID-related shutdowns were particularly detrimental to our vulnerable student and technician staffing. The unexpected departure of some of these young researchers during and after COVID significantly delayed the project.

Partnering with ISFH for Si IBC bottom subcells was instrumental to the project, and an exemplary international collaboration. Partnering with Alta Devices for large area III-V subcell was problematic because they unexpectedly went out of business, but we were able to pivot to working with SolAero to obtain these resources.

9. Path Forward:

The research conducted in this program is one building block for the new FY22-24 Tandem Photovoltaics Core Program (Award DE-00038266). The understanding of integration losses and modeling capabilities are critical to the development of perovskite/Si tandems and understanding the energy yield of multiple tandem architectures.

10. Inventions, Patents, Publications, and Other Results:

This project resulted in many peer reviewed publications [1-26] with one still under review [27]. The methods of 2T and 3T modeling and energy yield analysis have been published as open-source software [28]. One patent has been issued [29].

11. References:

1. J. Buencuerpo, J. F. Geisz, M. A. Steiner and A. C. Tamboli, "Enabling ultrathin III-V solar cells using dual photonic crystals." *Proceedings of the 46th IEEE PVSC*, Chicago, IL, p. 0001 (2019). https://doi.org/10.1109/PVSC40753.2019.8980639
2. M. Rienäcker, E. L. Warren, M. Schnabel, H. Schulte-Huxel, R. Niepelt, R. Brendel, P. Stradins, A. Tamboli and R. Peibst, "Back-contacted bottom cells with three terminals: Maximizing power extraction from current-mismatched tandem cells." Prog. Photovolt: Res. Appl. **27**, p. 410 (2019). https://doi.org/10.1002/pip.3107
3. M. Rienacker, E. L. Warren, T. F. Wietler, P. Stradins, A. C. Tamboli and R. Peibst, "Three-Terminal Bipolar Junction Bottom Cell as Simple as PERC: Towards Lean Tandem Cell Processing." *Proceedings of the 46th Photovoltaic Specialists Conference*, Chicago, IL, p. (2019). https://doi.org/10.1109/PVSC40753.2019.8980645
4. P. Stradins, M. Rienäcker, R. Peibst, A. Tamboli and E. Warren, "A simple physical model for three-terminal tandem cell operation." *Proceedings of the 46th IEEE PVSC*, p. 2176 (2019). https://doi.org/10.1109/PVSC40753.2019.8980595
5. K. T. VanSant, J. Simon, J. F. Geisz, E. L. Warren, K. L. Schulte, A. J. Ptak, M. S. Young, M. Rienäcker, H. Schulte-Huxel, R. Peibst and A. C. Tamboli, "Toward Low-Cost 4-Terminal GaAs//Si Tandem Solar Cells." ACS Applied Energy Materials **2**, p. 2375 (2019). https://doi.org/10.1021/acsaem.9b00018
6. M. H. Zehender, I. Garcia, S. A. Svatak, M. A. Steiner, P. Garcia-Linares, E. Warren, A. Tamboli and A. Marti, "Demonstrating the GaInP/GaAs Three-Terminal Heterojunction Bipolar Transistor Solar Cell." Proceedings of the 46th IEEE PVSC, Chicago, IL, p. (2019). https://doi.org/10.1109/PVSC40753.2019.8980563
7. J. Buencuerpo, J. F. Geisz, M. S. Young, T. R. Klein, E. L. Warren and A. C. Tamboli, "Stringing monolithic three terminal III-V tandems." *Proceedings of the 47th IEEE Photovoltaic Specialists Conference*, Calgary, p. 266 (2020). https://doi.org/10.1109/PVSC45281.2020.9300914
8. J. Buencuerpo, M. A. Steiner and A. C. Tamboli, "Optically-thick 300 nm GaAs solar cells using adjacent photonic crystals." Opt Express **28**, p. 13845 (2020). https://doi.org/10.1364/OE.391737
9. Y. Liu, Y. Li, Y. Wu, G. Yang, L. Mazzarella, P. Procel-Moya, A. C. Tamboli, K. Weber, M. Boccard, O. Isabella, X. Yang and B. Sun, "High-Efficiency Silicon Heterojunction Solar Cells: Materials, Devices and Applications." Materals Science and Enginging: R: Reports **142**, p. 100579 (2020). https://doi.org/10.1016/j.mser.2020.100579
10. W. E. McMahon, H. Schulte-Huxel, J. Buencuerpo, M. Young, T. R. Klein, J. F. Geisz, A. Tamboli and E. Warren, "Voltage-Matched Strings using 3-Terminal Tandems: Fundamentals and End Losses." *Proceedings of the 47th IEEE Photovoltaic Specialists Conference*, Calgary, p. (2020). https://doi.org/10.1109/PVSC45281.2020.9300569

11. M. Schnabel, H. Schulte-Huxel, M. Rienäcker, E. L. Warren, P. F. Ndione, W. Nemeth, T. R. Klein, M. F. A. M. van Hest, J. F. Geisz, R. Peibst, P. Stradins and A. C. Tamboli, “Three-terminal III–V/Si tandem solar cells enabled by a transparent conductive adhesive.” Sustainable Energy & Fuels **4**, p. 549 (2020). https://doi.org/10.1039/C9SE00893D
12. E. L. Warren, W. E. McMahon, M. Rienäcker, K. T. VanSant, R. C. Whitehead, R. Peibst and A. C. Tamboli, “A Taxonomy for Three-Terminal Tandem Solar Cells.” ACS Energy Letters **5**, p. 1233 (2020). https://dx.doi.org/10.1021/acsenergylett.0c00068?ref=pdf
13. G. M. Wilson, M. M. Al-Jassim, W. K. Metzger, S. W. Glunz, P. J. Verlinden, G. Xiong, L. M. Mansfield, B. Stanbery, K. Zhu, Y. Yan, J. J. Berry, A. J. Ptak, F. Dimroth, B. M. Kayes, A. C. Tamboli, R. Peibst, K. Catchpole, M. O. Reese, C. S. Klinga, P. Denholm, M. Morjaria, M. G. Deceglie, J. M. Freeman, M. A. Mikofskit, D. C. Jordan, G. TmizhMani and D. B. Sulas-Kern, “The 2020 photovoltaic technologies roadmap.” Journal of Physics D: Applied Physics **53**, p. 493001 (2020). https://doi.org/10.1088/1361-6463/ab9c6a
14. M. H. Zehender, S. A. Svatek, M. A. Steiner, I. García, P. Linares and E. L. Warren, "Inverted GaInP/GaAs Three-Terminal Heterojunction Bipolar Transistor Solar Cell." *Proceedings of the 47th IEEE PVSC*, p. 1517 (2020). https://doi.org/10.1109/PVSC45281.2020.9301000
15. J. Buencuerpo, J. M. Llorens, J. M. Ripalda, M. A. Steiner and A. C. Tamboli, “Engineering the reciprocal space for ultrathin GaAs solar cells.” Optics & Laser Technology **142**, p. 107224 (2021). https://doi.org/10.1016/j.optlastec.2021.107224
16. J. Buencuerpo, T. E. Saenz, S. Theingi, M. Young, J. F. Geisz, E. L. Warren, M. A. Steiner and A. C. Tamboli, "Fabrication of quasi-random photonic crystals for ultrathin solar cells." *Proceedings of the 48th IEEE Photovoltaic Specialists Conference*, Fort Lauderdale, p. 1193 (2021). https://doi.org/10.1109/PVSC43889.2021.9518404
17. J. F. Geisz, J. Buencuerpo, W. E. McMahon, T. R. Klein, A. C. Tamboli and E. L. Warren, "Fabrication, Measurement, and Modeling of GaInP/GaAs Three-Terminal Cells and Strings." *Proceedings of the IEEE 48th Photovoltiac Specialists Conference*, Fort Lauderdale, p. 154 (2021). https://doi.org/10.1109/PVSC43889.2021.9518913
18. J. F. Geisz, W. E. McMahon, J. Buencuerpo, M. S. Young, M. Rienäcker, A. C. Tamboli and E. L. Warren, “Characterization of multiterminal tandem photovoltaic devices and their subcell coupling.” Cell Reports Physical Science **2**, p. 100677 (2021). https://doi.org/10.1016/j.xcrp.2021.100677
19. T. R. Klein, M. S. Young, A. C. Tamboli and E. L. Warren, “Lamination of transparent conductive adhesives for tandem solar cell applications.” Journal of Physics D: Applied Physics **54**, p. 184002 (2021). https://doi.org/10.1088/1361-6463/abe2c4
20. W. E. McMahon, H. Schulte-Huxel, J. Buencuerpo, J. F. Geisz, M. S. Young, T. R. Klein, A. C. Tamboli and E. L. Warren, “Homogenous Voltage-Matched Strings using 3-Terminal Tandem Solar Cells: Fundamentals and End Losses.” IEEE Journal of Photovoltaics **11**, p. 1078 (2021). https://doi.org/10.1109/JPHOTOV.2021.3068325
21. K. T. VanSant, A. C. Tamboli and E. L. Warren, “III-V-on-Si tandem Solar Cells.” Joule **5**, p. 514 (2021). https://doi.org/10.1016/j.joule.2021.01.010
22. R. C. Whitehead, K. T. VanSant, E. L. Warren, J. Buencuerpo, M. Rienäcker, R. Peibst, J. F. Geisz and A. C. Tamboli, “Optimization of four terminal rear heterojunction GaAs on Si interdigitated back contact tandem solar cells.” Appl. Phys. Lett. **118**, p. 183902 (2021). https://doi.org/10.1063/5.0049097
23. E. Antolin, M. H. Zehender, S. Svatek, M. A. Steiner, M. Martinez, I. Garcia, P. Garcia-Linares, E. L. Warren, A. C. Tamboli and A. Marti, “Progress in three-terminal heterojunction bipolar transistor solar cells.” Progress in Photovoltaics **30**, p. 843 (2022). https://doi.org/10.1002/pip.3536
24. J. Buencuerpo, T. E. Saenz, M. Steger, M. Young, E. L. Warren, J. F. Geisz, M. A. Steiner and A. C. Tamboli, “Efficient light-trapping in ultrathin GaAs solar cells using quasi-random photonic crystals.” Nano Energy **96**, p. 107080 (2022). https://doi.org/10.1016/j.nanoen.2022.107080
25. J. F. Geisz, W. E. McMahon, J. Buencuerpo, M. Rienäcker, A. C. Tamboli and E. L. Warren, "Subcell Coupling in Tandem Solar Cells: Measurements and Modeling." Proceedings of the TandemPV2022, Freiburg, p. (2022). https://www.nrel.gov/docs/fy22osti/82229.pdf
26. K. VanSant, E. L. Warren, J. F. Geisz, T. R. Klein, S. Johnston, W. E. McMahon, H. Schulte-Huxel, M. Rienäcker, R. Peibst and T. C. Tambo, “A performance comparison between GaInP-on-Si and GaAs-on-Si 3-terminal tandem solar cells.” iScience **25**, p. 104950 (2022). https://doi.org/10.1016/j.isci.2022.104950

27. W. E. McMahon, J. F. Geisz, J. Buencuerpo and E. L. Warren, “A Framework for Comparing the Energy Production of Photovoltaic Modules using 2-, 3-, and 4-Terminal Tandem Cells.” Sustainable Energy and Fuels **7**, p. 461 (2023). https://doi.org/10.1039/D2SE01167K
28. *PVcircuit software*, J. F. Geisz, E. L. Warren and W. E. McMahon, 2022, https://github.com/NREL/PVcircuit, https://doi.org/10.11578/dc.20220518.1.
29. P. Stradins, E. L. Warren and A. C. Tamboli, "Tandem Module Unit", USPTO, Application # 16/995,378, Publication #US 2021/0050466, 2021
30. S. Essig, S. Ward, M. A. Steiner, D. J. Friedman, J. F. Geisz, P. Stradins and D. L. Young, “Progress towards a 30% efficient GaInP/Si tandem solar cell.” Energy Procedia **77**, p. 464 (2015). http://dx.doi.org/10.1016/j.egypro.2015.07.066
31. J. M. Gee, R. Y. Loo, G. S. Kamath and K. R.C., "A GaAs / Silicon mechanically stacked multijunction solar cell." *Proceedings of the IEEE Photovoltaic Specialists Conference*, p. 546 (1985).
32. Z. Yu, M. Leilaeioun and Z. Holman, “Selecting tandem partners for silicon solar cells.” Nature Energy **1**, p. 16137 (2016). https://doi.org/10.1038/NENERGY.2016.137
33. Z. J. Yu, J. V. Carpenter and Z. C. Holman, “Techno-economic viability of silicon-based tandem photovoltaic modules in the United States.” Nature Energy **3**, p. 747 (2018). https://doi.org/10.1038/s41560-018-0201-5
34. G. W. P. Adhyaksa, E. Johlin and E. C. Garnett, “Nanoscale Back Contact Perovskite Solar Cell Design for Improved Tandem Efficiency.” Nato Lett. **17**, p. 5206 (2017). https://doi.org/10.1021/acs.nanolett.7b01092
35. T. Nagashima, K. Okumra, K. Murata and Y. Kimura, "Three-terminal tandem solar cells with a back-contact type bottom cell." *Proceedings of the 28th IEEE PVSC*, Anchorage, AK, p. 1193 (2000). https://doi.org/10.1109/PVSC.2000.916102
36. E. L. Warren, M. G. Deceglie, M. Rienäcker, R. Peibst, A. Tamboli and P. Stradins, “Maximizing tandem solar cell power extraction using a three-terminal design.” Sustainable Energy & Fuels **2**, p. 1141 (2018). https://doi.org/10.1039/C8SE00133B
37. J. M. Gee, “A comparison of different module configurations for multi-band-gap solar cells.”, Solar Cells **24**, p. 147 (1988).
38. H. Schulte-Huxel, D. Friedman and A. Tamboli, “String-Level Modeling of Two, Three, and Four Terminal Si-Based Tandem Modules.” IEEE Journal of Photovoltaics **8**, p. 1370 (2018). https://doi.org/10.1109/JPHOTOV.2018.2855104
39. H. Schulte-Huxel, E. L. Warren, M. Schnabel, P. Stradins, D. Friedman and T. C. Tambo, "III-V/Si tandem cell to module interconnection – comparison between different operation modes." *Proceedings of the Photovoltaic Specialists Conference*, p. 2543 (2017). https://doi.org/10.1109/PVSC.2017.8366558
40. F. Gota, M. Langenhorst, R. Schmager, J. Lehr and U. W. Paetzold, “Energy Yield Advantages of Three-Terminal Perovskite-Silicon Tandem Photovoltaics.” Joule **4**, p. 2387 (2020). https://doi.org/10.1016/j.joule.2020.08.021
41. S. Essig, Allebe, T. Remo, J. F. Geisz, M. A. Steiner, K. Horowitz, L. Barraud, J. S. Ward, M. Schnabel, A. Descoeudres, D. L. Young, M. Woodhouse, M. Despeisse, C. Ballif and A. Tamboli, “Raising the one-sun conversion efficiency of III–V/Si solar cells to 32.8% for two junctions and 35.9% for three junctions.” Nature Energy **2**, p. 17144 (2017). http://dx.doi.org/10.1038/nenergy.2017.144
42. T. R. Klein, B. G. Lee, M. Schnabel, E. L. Warren, P. Stradins, A. C. Tamboli and M. F. A. M. van Hest, “Transparent Conductive Adhesives for Tandem Solar Cells Using Polymer–Particle Composites.” ACS Applied Mater. Inferfaces **10**, p. 8086 (2018). https://pubs.acs.org/doi/abs/10.1021/acsami.8b00175
43. M. J. Ludowise, "Three-junction solar cell", Application # 669,273, Publication #4,575,576, 1986
44. J. M. Gee, "Voltage-matched configurations for multijunction solar cells." *Proceedings of the Proceedings of the 19th IEEE Photovoltaic Specialists Conference*, New Orleans, p. 987 (1987).
45. S. M. Bedair, “AlGaAs tunnel diode.” J. Appl. Phys. **50**, p. 7267 (1979).
46. S. M. Bedair, J. A. Hutchby, J. Chiang, M. Simons and J. R. Hauser, "AlGaAs/GaAs High Efficiency Cascade Solar Cells." *Proceedings of the 15th IEEE Photovoltaic Specialists Conference*, p. 21 (1981).

47. M. Schnabel, M. Rienäcker, E. L. Warren, J. F. Geisz, R. Peibst, P. Stradins and A. C. Tamboli, “Equivalent perfomance in three-terminal and four-terminal tandem solar cells.” IEEE Journal of Photovoltaics **8**, p. 1584 (2018). https://doi.org/10.1109/JPHOTOV.2018.2865175
48. J. M. Ripalda, J. Buencuerpo and I. Garcia, “Solar cell designs by maximizing energy production based on machine learning clustering of spectral variations.” Nature Communications **9**, p. 5126 (2018). https://doi.org/10.1038/s41467-018-07431-3
49. J. M. Ripalda, D. Chemisana, J. M. Llorens and I. Garcia, “Location-Specific Spectral and Thermal Effects in Tracking and Fixed Tilt Photovoltaic Systems.” iScience **23**, p. 101634 (2020). https://doi.org/10.1016/j.isci